

Safe Imitation Learning of Nonlinear Model Predictive Control for Flexible Robots

Shamil Mamedov*

SHAMIL.MAMEDOV@KULEUVEN.BE

*MECO Research Team, KU Leuven, 3000 Leuven, Belgium
DMMS Lab, Flanders Make, 3001 Leuven, Belgium*

Rudolf Reiter*

RUDOLF.REITER@IMTEK.UNI-FREIBURG.DE

*Department of Microsystems Engineering
University Freiburg, 79110 Freiburg, Germany*

Moritz Diehl

MORITZ.DIEHL@IMTEK.UNI-FREIBURG.DE

*Department of Microsystems Engineering, Department of Mathematics
University Freiburg, 79110 Freiburg, Germany*

Jan Swevers

JAN.SWEVERS@KULEUVEN.BE

*MECO Research Team, KU Leuven, 3000 Leuven, Belgium
DMMS Lab, Flanders Make, 3001 Leuven, Belgium*

Editors: R. Firoozi, N. Mehr, E. Yel, R. Antonova, J. Bohg, M. Schwager, M. Kochenderfer

Abstract

Flexible robots may overcome the industry’s major problems: safe human-robot collaboration and increased load-to-mass ratio. However, oscillations and high dimensional state space complicate the control of flexible robots. This work investigates nonlinear model predictive control (NMPC) of flexible robots – for simultaneous planning and control – modeled via the rigid finite element method. Although NMPC performs well in simulation, computational complexity prevents its deployment in practice. We show that imitation learning of NMPC with neural networks as function approximator can massively improve the computation time of the controller at the cost of slight performance loss and, more critically, loss of safety guarantees. We leverage a *safety filter* formulated as a simpler NMPC to recover safety guarantees. Experiments on a simulated three degrees of freedom flexible robot manipulator demonstrate that the average computational time of the proposed safe approximate NMPC controller is 3.6 ms while of the original NMPC is 11.8 ms. Fast and safe approximate NMPC might facilitate the industry’s adoption of flexible robots and new solutions for similar problems, e.g., deformable object manipulation and soft robot control.

Keywords: flexible robots, rigid finite element method, NMPC, imitation learning, safety filter

1. Introduction

In recent years flexible robots have been drawing more attention as they might hold the key to the industry’s significant problems. These problems include increasing the load-to-mass ratio and making robots intrinsically safer to facilitate human-robot collaboration. The main reason why flexible robots have yet to be adopted is the flexibility that causes oscillations and static deflections, complicating modeling and control.

. * These authors contributed equally.

Flexible robots have an infinite number of degree of freedom (DOF) and are governed by non-linear partial differential equations (PDE). Discretization converts PDE into ordinary differential equations (ODE), making them suitable for control and trajectory planning. There are three main methods for discretizing a flexible link: the assumed mode method (AMM) (Book, 1984; Green and Sasiadek, 2004), the finite element method (FEM) (Sunada and Dubowsky, 1981; Shabana, 2020) and the lumped parameter method (LPM) (Yoshikawa and Hosoda, 1996; Franke et al., 2009; Stauffer and Gattringer, 2012; Moberg et al., 2014). All the methods generally assume small deformations and use the linear theory of elasticity. The FEM is the most accurate among the three but results in a higher number of differential equations. The AMM is often used for one DOF flexible robots; for robots with higher DOF, the choice of boundary conditions becomes nontrivial (Heckmann, 2010). The LPM is the simplest among the three, but tuning the parameters of such models takes much work. In this paper, we leverage the LPM following formulation defined in Wittbrodt et al. (2007), where the method is called the modified rigid FEM (MRFEM). The Section 2 describes the method in detail.

Many control methods have been proposed for controlling flexible robots, including optimal control methods. Green and Sasiadek (2004) applied LQR for trajectory tracking control of a two-link flexible robot using linearized dynamics. Silva et al. (2020) used model predictive control (MPC) to control a single-link flexible robot, while Boscaroli et al. (2010) used MPC to control four-link flexible mechanisms. In both cases, the authors linearized the dynamics and used linear MPC. Indeed, designing fast nonlinear model predictive control (NMPC) is challenging given the high dimensional dynamics of flexible robots.

To make NMPC available for a broader range of systems, there have been attempts in the last two decades to approximate NMPC with neural networks (NN) Grancharova and Johansen (2012). Nubert et al. (2020) proposed using supervised learning to approximate robust NMPC, while Carius et al. (2020) proposed a policy search method guided by NMPC without safety considerations. To ensure that the approximate NMPC provides safe inputs (does not violate constraints), Nubert et al. (2020) leveraged a statistical validation technique to obtain safety guarantees. The authors reported that the validation process is time-consuming. In general, approximating NMPC with NN fits under the umbrella of imitation learning (IL). Brunke et al. (2022) discuss various methods for ensuring the safety of learning methods. One particular approach to guarantee the safety of a learned policy is the safety filter (SF) (Wabersich and Zeilinger, 2021). SF is an MPC scheme that receives a candidate input and verifies if it can drive the system to a safe terminal set after applying the candidate input. If the answer is positive, the input is applied to the system; otherwise, it is modified as little as possible to ensure safety. Vinod et al. (2022) successfully used SF for a multi-agent drone setup that was trained with reinforcement learning (RL). To the best of the authors knowledge, this paper is the first that investigates whether IL combined with SF can replace NMPC for safe regulation and trajectory tracking control of flexible robots. We show that our particular implementation successfully speeds up computation time of the controller, filters unsafe controls while operating close to the expert’s performance.

The paper is organized as follows: Section 2 describes the setup, Section 3 formulates NMPC while Section 4 describes IL as a tool to approximate NMPC. Section 5 presents simulation studies of several controllers for regulation and trajectory tracking and discusses the results. Finally, in Section 6, we make concluding remarks.

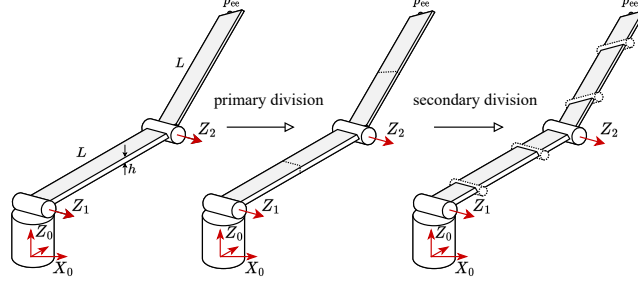


Figure 1: Schematic representation of the setup and of the discretization method.

2. Setup

The simulation setup is a three DOF serial manipulator, as shown in Fig. 1, which was inspired by flexible robots TUDOR (Malzahn et al., 2010) and ELLA (Stauffer and Gattringer, 2012). The first link is rigid; the second and third links are flexible and have the same dimensions and material properties. We assume that joints are rigid and directly actuated, i.e., actuators do not have a gear-box. Available measurements are actuated joints positions and velocities, and the end effector (EE) position to monitor elastic deflections.

2.1. Modeling

For modeling the robot, we utilize MRFEM; it, first, divides the flexible links into n_{seg} segments and lumps their spring and damping properties at one point, e.g., in the geometrical center of the segment. Then, MRFEM isolates so-called rigid finite elements (rfes) between massless passive joints (spring-damper elements), see Fig. 1. Mechanics textbooks contain ready-to-use formulas for computing inertial properties of the rfes, and spring and damper coefficients for simple geometries. For complex geometries, however, CAD software should be used.

For deriving the equations of motion of a flexible manipulator using the Lagrange method (Sciavicco and Siciliano, 2001, Ch. 7), let $\mathbf{q} = (\mathbf{q}_a; \mathbf{q}_p)$ denote the vector of joint angles with $\mathbf{q}_a \in \mathbb{R}^3$ being the vector of active joint angles and $\mathbf{q}_p \in \mathbb{R}^{2n_{\text{seg}}}$ being the vector of passive joint angles. Passive joints are generally chosen as spherical joints to represent compliance in all directions (two bending deformations and a torsional deformation). For some geometries, as in our case, compliance in one direction dominates compliance in other directions. Reducing the model by modeling flexibility only along the most compliant direction is beneficial in such cases. In the setup, we only model the bending about axes Z_1 and Z_2 , as shown in Fig. 1. The kinetic energy K , the potential energy P and the dissipation D functions of the manipulator are:

$$K(\mathbf{q}, \dot{\mathbf{q}}) = \frac{1}{2} \dot{\mathbf{q}}^\top \mathbf{M}(\mathbf{q}) \dot{\mathbf{q}}, \quad P(\mathbf{q}) = \frac{1}{2} \mathbf{q}^\top \mathbf{K} \mathbf{q} + \sum_{i=0}^{n_{\text{rb}}} m_i g_0 p_{C_i}, \quad D(\dot{\mathbf{q}}) = \frac{1}{2} \dot{\mathbf{q}}^\top \mathbf{D} \dot{\mathbf{q}}, \quad (1)$$

where $n_{\text{rb}} = 1 + 2(n_{\text{seg}} + 1)$ is the number of rigid bodies, $\mathbf{M} \in \mathbb{R}^{n_{\text{rb}} \times n_{\text{rb}}}$ is the symmetric inertia matrix; $\mathbf{K} \in \mathbb{R}^{n_{\text{rb}} \times n_{\text{rb}}}$ and $\mathbf{D} \in \mathbb{R}^{n_{\text{rb}} \times n_{\text{rb}}}$ are the constant diagonal stiffness and damping matrices, respectively; m_i and $\mathbf{p}_{C_i} \in \mathbb{R}^3$ are i -th links mass and center of mass, respectively; $\mathbf{g}_0 = [0 \ 0 \ -9.81]^\top \text{ m/s}^2$ is the gravity acceleration vector. Applying the Lagrange method yields the final expression for the flexible manipulator dynamics discretized using MRFEM

$$\mathbf{M}(\mathbf{q}) \ddot{\mathbf{q}} + \mathbf{C}(\mathbf{q}, \dot{\mathbf{q}}) \dot{\mathbf{q}} + \mathbf{K} \mathbf{q} + \mathbf{D} \dot{\mathbf{q}} + \mathbf{g}(\mathbf{q}) = \mathbf{B} \boldsymbol{\tau}, \quad (2)$$

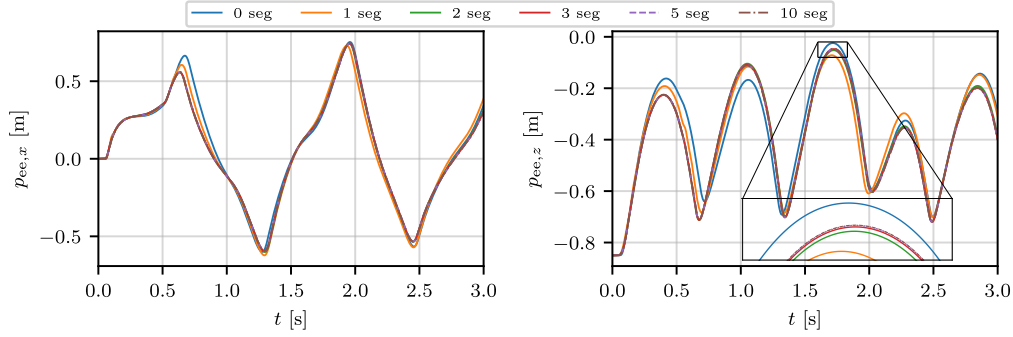


Figure 2: EE positions x and z simulated for a different number of segments n_{seg} .

where $\mathbf{C} \in \mathbb{R}^{n_{\text{rb}} \times n_{\text{rb}}}$ is the matrix of centrifugal and Coriolis forces, $\mathbf{g} \in \mathbb{R}^{n_{\text{rb}}}$ is the vector of gravitational forces, $\mathbf{B} \in \mathbb{R}^{n_{\text{rb}} \times 3}$ is the constant control jacobian and $\boldsymbol{\tau} \in \mathbb{R}^3$ is the torque vector. The model is converted to state space form by defining $\mathbf{x} := (\mathbf{q}; \dot{\mathbf{q}})$ and $\mathbf{u} := \boldsymbol{\tau}$

$$\dot{\mathbf{x}} = \mathbf{f}(\mathbf{x}, \mathbf{u}, n_{\text{seg}}) = (\dot{\mathbf{q}}; \mathbf{M}(\mathbf{q})^{-1} \{ \mathbf{B}\boldsymbol{\tau} - \mathbf{C}(\mathbf{q}, \dot{\mathbf{q}})\dot{\mathbf{q}} - \mathbf{K}\mathbf{q} - \mathbf{D}\dot{\mathbf{q}} - \mathbf{g}(\mathbf{q}) \}). \quad (3)$$

The output map of the system is $\mathbf{y} = \mathbf{h}(\mathbf{x}) = (\mathbf{q}_a; \dot{\mathbf{q}}_a; \mathbf{p}_{\text{ee}})$ where \mathbf{p}_{ee} is the EE position.

2.2. Simulation and discretization

Roboticians favor MRFEM because existing efficient tools for rigid-body dynamics can be reused: the articulated body algorithm (ABA) for forward dynamics and the recursive Newton-Euler algorithm (RNEA) for the inverse dynamics (Featherstone, 2014). In this paper, we use ABA for the forward dynamics and the forward path of the RNEA for the forward kinematics, both generated by Pinocchio (Carpentier et al., 2019) as CasADi (Andersson et al., 2019) functions.

ODE (3) is stiff; commonly used explicit fixed-step integrators in optimal control, e.g. 4-th order Runge-Kutta (RK4) integrator, quickly diverge. Implicit integrators, however, can accurately integrate (3) at a higher computational cost. In this paper, for simulation, we use the backward differentiation formula implemented in CVODES (Hindmarsh et al., 2005) with specified absolute and relative tolerances. As ground truth dynamics, we consider the model with $n_{\text{seg}} = 10$.

The critical aspect of any discretization method, including MRFEM is the choice of n_{seg} . Finer discretization, on the one hand, yields a better approximation of the natural frequencies of the flexible links, but, on the one hand, it yields a high dimensional state-space model of the form (3). Figure 2 shows the comparison between models with different n_{seg} in terms of x and z positions of the EE. All the models were initialized with equivalent initial states and were excited with two square wave signals: first, joint three with an amplitude of 5 Nm and a duration of 0.03 s; 0.42 s later, joint two with an amplitude of 10 Nm and a duration of 0.04 s. EE positions predicted by models with $n_{\text{seg}} = 0$ (rigid body approximation) and $n_{\text{seg}} = 1$ are noticeably different compared with finer discretized models. The EE position predictions of the model with just two segments approach the "true" (of the model with $n_{\text{seg}} = 10$) EE position. This result is consistent with the validation of MRFEM from Wittbrodt et al. (2007), Ch. 6, and indicates that a discretization as coarse as two segments might be sufficient for control purposes. Subsection 5.2 further investigates model complexity but from the the controller performance perspective.

3. Nonlinear model predictive control

We use NMPC to solve an optimal control problem for regulation around an EE goal position and refer to it as expert policy. We formulate it as a general nonlinear program (NLP), as detailed in the following section.

3.1. NLP Formulation

In order to formulate the NLP for solving the NMPC problem, we use multiple shooting: we discretize the trajectory into $N-1$ intervals, leading to the state decision variables $\mathbf{X} = [\mathbf{x}_0, \dots, \mathbf{x}_N] \in \mathbb{R}^{n_x \times N}$ and the control decision variables $\mathbf{U} = [\mathbf{u}_0, \dots, \mathbf{u}_{N-1}] \in \mathbb{R}^{n_u \times N-1}$. Additionally, we use algebraic variables $\mathbf{Z} = [\mathbf{z}_0, \dots, \mathbf{z}_N] \in \mathbb{R}^{n_z \times N}$ for the EE position of the robot. In the cost function, we penalize the deviation from reference EE positions $\mathbf{z}_0^{\text{ref}}, \dots, \mathbf{z}_N^{\text{ref}}$, reference states $\mathbf{x}_0^{\text{ref}}, \dots, \mathbf{x}_N^{\text{ref}}$ and reference torques $\mathbf{u}_0^{\text{ref}}, \dots, \mathbf{u}_{N-1}^{\text{ref}}$ using the squared L2 norm. The weight matrices of the squared L2 norms are $\mathbf{Q} = \text{diag}(\mathbf{w}) \in \mathbb{R}^{n_x \times n_x}$, $\mathbf{Q}_N \in \mathbb{R}^{n_x \times n_x}$, $\mathbf{R} = \text{diag}(\mathbf{r}) \in \mathbb{R}^{n_u \times n_u}$, $\mathbf{P} = \text{diag}(\mathbf{p}) \in \mathbb{R}^{n_z \times n_z}$ and $\mathbf{P}_N \in \mathbb{R}^{n_z \times n_z}$. Vector \mathbf{w} contains weights w_{q_a} for active joints positions, w_{q_p} for passive joint positions, $w_{\dot{q}_a}$ for active joint velocities and $w_{\dot{q}_p}$ for passive joint velocities. We formulate constraints for joint velocities and obstacles using slack variables $\Sigma = [\sigma_0, \dots, \sigma_N]^\top \in \mathbb{R}^{2 \times N}$, with $\sigma_k = [\sigma_k^{\dot{q}} \ \sigma_k^{\text{obs}}]^\top \in \mathbb{R}^2$. Slack variables are penalized in the cost function by L1- and squared L2-norms (by weights $\mathbf{s} \in \mathbb{R}^2$ and $\mathbf{S} \in \mathbb{R}^{2 \times 2}$, respectively).

$$\begin{aligned} L(\mathbf{X}, \mathbf{U}, \mathbf{Z}, \Sigma) = & \sum_{k=0}^{N-1} \left\| \mathbf{x}_k - \mathbf{x}_k^{\text{ref}} \right\|_{\mathbf{Q}}^2 + \left\| \mathbf{u}_k - \mathbf{u}_k^{\text{ref}} \right\|_{\mathbf{R}}^2 + \left\| \mathbf{z}_k - \mathbf{z}_k^{\text{ref}} \right\|_{\mathbf{P}}^2 + \left\| \sigma_k \right\|_{\mathbf{S}}^2 + \left\| \sigma_k \right\|_{1, \mathbf{s}} + \\ & \left\| \mathbf{x}_N - \mathbf{x}_N^{\text{ref}} \right\|_{\mathbf{Q}_N}^2 + \left\| \mathbf{z}_N - \mathbf{z}_N^{\text{ref}} \right\|_{\mathbf{P}_N}^2 + \left\| \sigma_N \right\|_{\mathbf{S}}^2 + \left\| \sigma_N \right\|_{1, \mathbf{s}}. \end{aligned} \quad (4)$$

We use a four-stage implicit RK method with a sampling time Δt to discretize the continuous time system dynamics (3), leading to the equality constraints $\mathbf{0} = \mathbf{F}(\mathbf{x}_{k+1}, \mathbf{x}_k, \mathbf{u}_k)$. We use forward kinematics $\mathbf{p}_{\text{EE}} = \mathbf{P}^{\text{fwd}}(\mathbf{x})$ to define the algebraic equation $\mathbf{z}_k = \mathbf{P}^{\text{fwd}}(\mathbf{x}_k)$. We encode obstacle constraints as box constraints for the algebraic states with an upper bound $\bar{\mathbf{z}}^{\text{tr}}$ and a lower bound $\underline{\mathbf{z}}^{\text{tr}}$. Control upper bounds $\bar{\mathbf{u}}$, control lower bounds $\underline{\mathbf{u}}$, state upper bounds $\bar{\mathbf{x}}^{\text{tr}}$ and state lower bounds $\underline{\mathbf{x}}^{\text{tr}}$ are used to formulate box constraints on input torques and joint velocities, respectively. To avoid constraint violation due to noisy measurements, we perform a simple heuristic-based constraint tightening. In particular, based on the knowledge about the measurement noise, we assume a safety margin $\delta_x = [\delta_q^\top \ \delta_{\dot{q}}^\top]^\top \in \mathbb{R}^x$ for the state constraints $\bar{\mathbf{x}} = \bar{\mathbf{x}}^{\text{tr}} - \delta_x$, $\underline{\mathbf{x}} = \underline{\mathbf{x}}^{\text{tr}} + \delta_x$, and δ_z for the EE position constraints $\bar{\mathbf{z}} = \bar{\mathbf{z}}^{\text{tr}} - \delta_z$, $\underline{\mathbf{z}} = \underline{\mathbf{z}}^{\text{tr}} + \delta_z$. By choosing generous safety margins we could avoid a more sophisticated robust NMPC formulation. Since the optimization problem can only be formulated for a finite horizon, a control invariant terminal set $S^t(x, z)$ is included, where we set

the joint velocities to zero. With the estimated state $\hat{\mathbf{x}}$, the final nonlinear program reads as

$$\underset{\mathbf{X}, \mathbf{U}, \mathbf{Z}, \Sigma}{\text{minimize}} \quad L(\mathbf{X}, \mathbf{U}, \mathbf{Z}, \Sigma) \quad (5a)$$

$$\text{subject to} \quad \mathbf{x}_0 = \hat{\mathbf{x}}, \quad \Sigma \geq 0, \quad (\mathbf{x}_N, \mathbf{z}_N) \in S^t, \quad (5b)$$

$$\mathbf{0} = \mathbf{F}(\mathbf{x}_{k+1}, \mathbf{x}_k, \mathbf{u}_k), \quad k = 0, \dots, N-1, \quad (5c)$$

$$\mathbf{z}_k = \mathbf{P}^{\text{fwd}}(\mathbf{x}_k), \quad k = 0, \dots, N, \quad (5d)$$

$$\underline{\mathbf{x}} - \sigma_k^{\dot{q}} \leq \mathbf{x}_k \leq \bar{\mathbf{x}} + \sigma_k^{\dot{q}}, \quad k = 0, \dots, N, \quad (5e)$$

$$\underline{\mathbf{z}} - \sigma_k^{\text{ref}} \leq \mathbf{z}_k \leq \bar{\mathbf{z}} + \sigma_k^{\text{ref}}, \quad k = 0, \dots, N, \quad (5f)$$

$$\underline{\mathbf{u}} \leq \mathbf{u}_k \leq \bar{\mathbf{u}}, \quad k = 0, \dots, N-1. \quad (5g)$$

3.2. Safety Filter

As we aim for approximating NMPC with a NN, safety w.r.t. the constraints in (5) cannot be guaranteed directly. [Wabersich and Zeilinger \(2021\)](#) propose an MPC-based policy $\pi^s : \mathbb{R}^{n_u} \rightarrow \mathbb{R}^{n_u}$ that projects the NN output $\mathbf{u}^{\text{NN}} \in \mathbb{R}^{n_u}$ to a safe control $\mathbf{u}^s = \pi^s(\mathbf{x}^s, \mathbf{u}^{\text{NN}}) \in \mathcal{U}^s \subseteq \mathbb{R}^{n_u}$. The safe set \mathcal{U}^s is defined as in (5g) for a possibly simpler discrete-time system model $\mathbf{x}_{i+1}^s = \mathbf{F}^s(\mathbf{x}_i^s, \mathbf{u}_i^s)$ with states \mathbf{x}^s and controls \mathbf{u}^s . Constraint satisfaction for states is expressed via the set membership of state variables $\mathbf{x}^s \in \mathcal{X}^s$ (5e), algebraic variables $\mathbf{z}^s \in \mathcal{Z}^s$ (5f), and for controls via $\mathbf{u}^s \in \mathcal{U}^s$. The safety filter solves the optimization problem (5) but with the cost function $\|\mathbf{u}_0^s - \mathbf{u}^{\text{NN}}\|_{\mathbf{R}^s}^2$ and decision variables $\mathbf{X}^s, \mathbf{U}^s, \mathbf{Z}^s, \Sigma^s$. It takes the first control \mathbf{u}_0^{s*} of the optimal solution $(\mathbf{X}^{s,*}, \mathbf{U}^{s,*})$ as filter output $\mathbf{u}^s := \mathbf{u}_0^{s*}$.

4. Imitation Learning

We aim at imitating the expert policy π^* , i.e., NMPC, by training a NN. Due to the violation of the i.i.d. assumption of sequential prediction problems, purely supervised learning performs poorly ([Ross et al., 2011](#)). One approach that leverages this problem and has shown superior performance in practice is named *DAGger* (Data Aggregation [Ross et al. \(2011\)](#)). It alternates between roll-outs by the neural network to aggregate states to dataset \mathcal{D} and queries the expert policy on those visited states. Thereafter, it performs supervised learning with an L2-loss function on the policy output (torques) for obtaining a trained policy π_i in iteration i . Consequently, [Ross et al. \(2011\)](#) showed that training samples for supervised learning are efficiently sampled. We use *DAGger* for IL, where we train for M episodes and collect n_0 state-action pairs in an initial phase and n_1 state-action pairs in each episode thereafter.

5. Experiments

5.1. State estimation

Since the number of segments n_{seg} of the model used for simulation differs from the n_{seg} of a control model and we simulate measurement noise, a state estimator is needed to infer the states of the control model from outputs \mathbf{y} of the simulation model. To this end, we implemented a commonly used discrete-time extended Kalman filter (EKF), which uses a model of form (3). We discretized the estimation model (which is the same as the control model) using the fixed-step implicit Radau

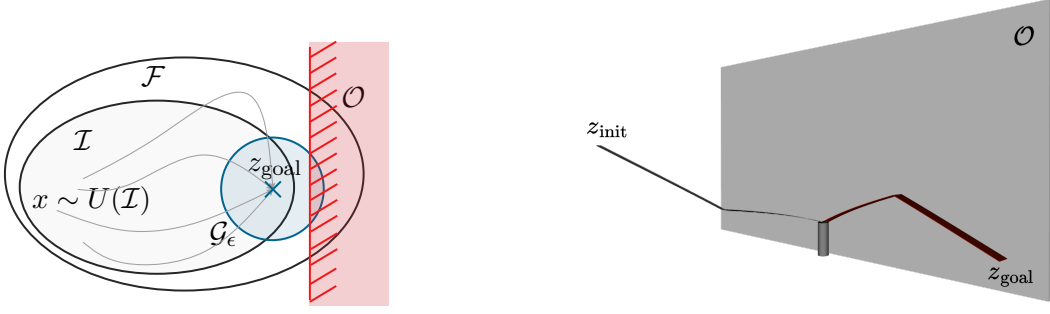


Figure 3: On the left, a sketch of the sets for the defined task is shown. The right image shows the rendered robot in the simulation environment with the goal location close to the safety-critical wall constraint.

collocation method; the linearization of the model is performed through automatic differentiation available in CasADi.

5.2. Model complexity comparison for NMPC

To analyze the influence of the model fidelity, i.e., the number of segments on the controller performance, we compared the NMPC for $n_{\text{seg}} = \{0, 1, 2, 3, 5, 10\}$. For $\{0, 1\}$ segments, the solver did not converge and for ten segments, the computation time is unacceptably long. We evaluate the performance of a controller by the path-length $d_{\mathcal{G}_\epsilon}$ of the EE position and time taken from an initial state to reach a goal region $\mathcal{G}_\epsilon(\bar{\epsilon})$ and stay within it. We define $\mathcal{G}_\epsilon(\bar{\epsilon}) = \{z \in \mathbb{R}^n | (z - z_{\text{goal}})^\top (z - z_{\text{goal}}) \leq \bar{\epsilon}\}$ as a ball of radius $\bar{\epsilon}$ around the goal EE position. As shown in Tab. 2, the average mean computation time \bar{t}_{MPC} and the maximum computation time $t_{\text{MPC}}^{\text{max}}$ increase drastically with a higher number of segments: $n_{\text{seg}} = \{2, 3, 5\}$. However, the performance measured in the KPIs $t_{\mathcal{G}_\epsilon}$ and $d_{\mathcal{G}_\epsilon}$ does not significantly improve. Therefore, we selected $n_{\text{seg}} = 2$ as a compromise between performance and computation time for MPC for further use within IL framework.

5.3. Set-to-point motion

The setup (Fig. 3) of the first task includes a goal EE position z_{goal} that should be reached from a initial rest state sampled from an initial set

$$\mathcal{I} = \left\{ \mathbf{q} \in \mathbb{R}^{n_x} \left| \begin{bmatrix} -\frac{\pi}{2} - 0.1, -\frac{\pi}{4}, -\frac{\pi}{4} \end{bmatrix}^\top \leq \mathbf{q}_a^\top \leq \begin{bmatrix} -0.1, \frac{\pi}{4}, \frac{\pi}{4} \end{bmatrix}^\top, \mathbf{q}_p, \dot{\mathbf{q}} = \mathbf{0} \right. \right\}, \quad (6)$$

where \mathbf{q}_p is the equilibrium configuration of passive joints for a given configuration of active joints ($\mathbf{K}\mathbf{q} + \mathbf{g}(\mathbf{q}) = \mathbf{0}$). The initial set is a subset of the reachable set \mathcal{F} which is constrained by an obstacle set $\mathcal{O} = \{p_{\text{EE}} \in \mathbb{R}^{n_z} | p_{y,\text{EE}} \geq 0\}$, where $p_{y,\text{EE}}$ is the y-component of the EE.

We trained the NN agent using *Dagger* for $M = 30$ episodes and collected $14 \cdot 10^4$ training samples. Fig. 4 shows a return – the sum of rewards $r_i = \Delta t \|z_{\text{goal}} - z_i\|_2$ used purely for evaluation within training – and the L2 loss. The resulting trained NN achieves a massive improvement in the computation time compared with expert NMPC, as shown in Tab. 1. However, it violates constraints since the learned expert’s motion is *sliding* along constraints, thus making it difficult for the NN to

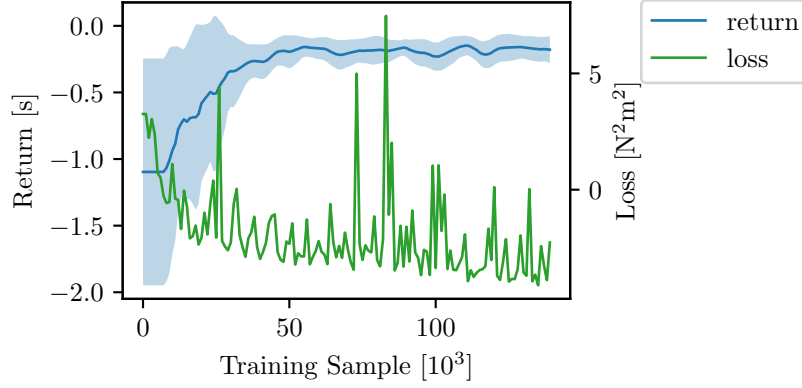


Figure 4: L2 loss and evaluation return (sum of distances from current EE position to the goal EE position) during IL of the expert policy.

approach	computation times [ms]			max. constr. violations		metric/KPI	$n_{\text{seg}} = 3$	$n_{\text{seg}} = 5$
	mean	std.	max.	\dot{q}_a [$\frac{\text{rad}}{\text{s}}$]	wall [cm]			
expert MPC ($N = 50$)	11.790	0.239	13.775	0.00	0.00	$d_{\mathcal{G}_\epsilon}/d_{\mathcal{G}_\epsilon}^*$	1.008	1.026
NN	0.091	0.001	0.095	4.02	4.46	$t_{\mathcal{G}_\epsilon}/t_{\mathcal{G}_\epsilon}^*$	0.955	0.974
NN + SF	3.619	0.258	7.304	0.00	0.00	$\bar{t}_{\text{MPC}}/\bar{t}_{\text{MPC}}^*$	1.653	2.95
MPC ($N = 10$)	2.701	0.098	3.511	0.00	3.51	$t_{\text{MPC}}^{\text{max}}/t_{\text{MPC}}^{\text{max},*}$	1.589	2.940
MPC ($N = 20$)	4.807	0.167	6.334	0.00	0.00			
MPC ($N = 40$)	9.540	0.247	11.679	0.00	0.00			
MPC ($N = 80$)	19.016	0.390	22.107	0.00	0.00			

Table 1: Computation times and constraint violations of MPC formulations with different horizon lengths, the trained NN and the NN including the SF.

Table 2: Performance comparison of NMPC controllers with different models. KPIs are measured with respect to KPIs of the NMPC with $n_{\text{seg}} = 2$, denoted with superscript $*$.

meet them precisely. The SF yields constraint satisfaction at the cost of increased computation time. Nevertheless, NN with SF is still much faster than the expert. For comparison, we implemented MPC with different horizons ($N = \{10, 20, 40, 80\}$). Shorter horizons decrease the computation time but may not maintain stability. Tab. 3 compares the performances of several controllers for different sizes ϵ of the goal region \mathcal{G}_ϵ as measured by selected KPIs. The expert’s performance on randomized initial states is given in absolute values, whereas other approaches are given relative to the expert’s performance, including the standard deviation over the experiments. For a larger goal region $\epsilon = 0.1\text{m}$, all the controllers perform similarly while for smaller values of ϵ the time to reach the goal increases compared with the expert for NN and SF+NN up to 25%, and the traveled path up to 6%. The SF+NN implementation performs slightly worse than the pure NN implementation, but yields a safety guarantee to our chosen robust constraints.

The time signals of a simulation run are plotted in Fig. 5, where the EE goal position is reached in approximately 1s. The NN violates the joint velocity constraint and nearly the EE y -position constraint. The SF successfully projects the outputs of the same NN to safe control, where constraints are respected.

	$\epsilon = 0.1$ [m]			$\epsilon = 0.05$ [m]			$\epsilon = 0.025$ [m]		
	f [%]	t_ϵ [s]	d_ϵ [m]	f [%]	t_ϵ [s]	d_ϵ (m)	f [%]	t_ϵ [s]	d_ϵ [m]
expert MPC ($N = 50$)	0	0.34 ± 0.15	0.72 ± 0.35	0	0.39 ± 0.14	0.79 ± 0.34	0	0.43 ± 0.12	0.82 ± 0.34
		$\frac{t_\epsilon}{t_\epsilon^{\text{exp}}}$	$\frac{d_\epsilon}{d_\epsilon^{\text{exp}}}$		$\frac{t_\epsilon}{t_\epsilon^{\text{exp}}}$	$\frac{d_\epsilon}{d_\epsilon^{\text{exp}}}$		$\frac{t_\epsilon}{t_\epsilon^{\text{exp}}}$	$\frac{d_\epsilon}{d_\epsilon^{\text{exp}}}$
NN	0	0.98 ± 0.13	1.01 ± 0.05	0	1.06 ± 0.14	1.04 ± 0.07	5	1.25 ± 0.18	1.06 ± 0.07
NN + SF	0	1.05 ± 0.08	1.00 ± 0.04	5	1.08 ± 0.16	1.01 ± 0.04	5	1.17 ± 0.27	1.02 ± 0.05
MPC ($N = 10$)	100	nan	nan	100	nan	nan	100	nan	nan
MPC ($N = 20$)	0	0.99 ± 0.04	0.99 ± 0.03	80	1.76 ± 1.10	1.11 ± 0.07	100	nan	nan
MPC ($N = 40$)	0	1.00 ± 0.01	1.00 ± 0.02	0	1.03 ± 0.10	1.01 ± 0.03	0	1.06 ± 0.14	1.01 ± 0.03
MPC ($N = 80$)	0	1.00 ± 0.00	1.00 ± 0.00	0	1.00 ± 0.02	1.00 ± 0.01	0	0.99 ± 0.03	1.00 ± 0.01

Table 3: Key performance indicators and the failure rate f of MPC formulations with different horizon lengths, the trained NN and the NN including the SF.

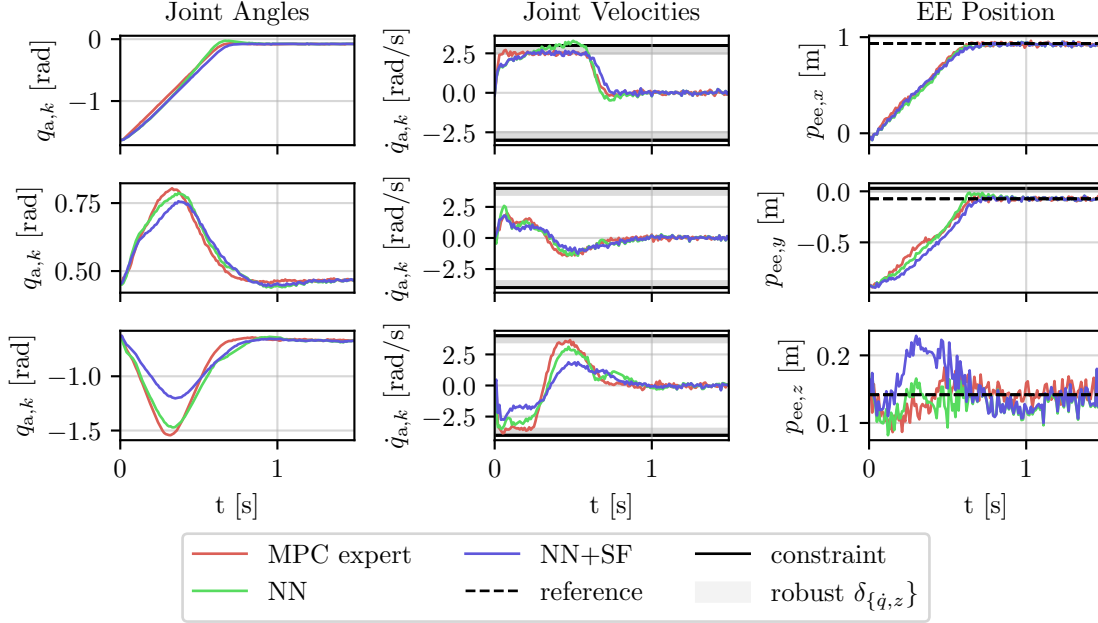


Figure 5: Simulation comparison of the expert MPC, the trained neural network (NN) and the trained NN with an addition of the safety filter (NN+SF). Despite good performance of the NN, it violates the joint velocity. The safety filter successfully avoids the constraint violation.

6. Conclusion

This work demonstrated that a three degree of freedom flexible robot manipulator, modeled using lumped parameter approach called the modified rigid finite element method, can be effectively controlled by NMPC. We used a high-fidelity simulator and compared NMPC formulations for different model complexities (discretizations of flexible links) and horizon lengths. We alleviated the problem of the rather high computation time of NMPC by approximating it with NN using imitation learning – reduced the computational load by a factor of 100. NN, however, does not give any safety guarantees. In order to recover safety, we combined the NN with a ”safety filter” formulated as a simple NMPC to project controls to a safe control set. The proposed approach can be easily

extended to trajectory tracking problems in flexible robotics and to control problems in soft robotics where robots are even more compliant and require even more complicated models.

Acknowledgments

The authors want to thank Daniele Ronzani for his helpful feedback.

This research was supported by DFG via Research Unit FOR 2401 and project 424107692 and by the EU via ELO-X 953348. This research was also supported by the Research Foundation Flanders (FWO-Vlaanderen) through SBO project Energy-efficient, Lightweight, safe Yet Strong manipulator Arm (ELYSA) for cobot applications (S001821N).

References

- Joel A E Andersson, Joris Gillis, Greg Horn, James B Rawlings, and Moritz Diehl. CasADi – A software framework for nonlinear optimization and optimal control. *Mathematical Programming Computation*, 11(1):1–36, 2019. doi: 10.1007/s12532-018-0139-4.
- Wayne J Book. Recursive lagrangian dynamics of flexible manipulator arms. *The International Journal of Robotics Research*, 3(3):87–101, 1984.
- Paolo Boscariol, Alessandro Gasparetto, and Vanni Zanotto. Model predictive control of a flexible links mechanism. *Journal of Intelligent and Robotic Systems*, 58(2):125–147, 2010.
- Lukas Brunke, Melissa Greeff, Adam W. Hall, Zhaocong Yuan, Siqi Zhou, Jacopo Panerati, and Angela P. Schoellig. Safe learning in robotics: From learning-based control to safe reinforcement learning. *Annual Review of Control, Robotics, and Autonomous Systems*, 5(1):411–444, 2022. doi: 10.1146/annurev-control-042920-020211. URL <https://doi.org/10.1146/annurev-control-042920-020211>.
- Jan Carius, Farbod Farshidian, and Marco Hutter. MPC-net: A first principles guided policy search. *IEEE Robotics and Automation Letters*, 5(2):2897–2904, apr 2020. doi: 10.1109/lra.2020.2974653.
- Justin Carpentier, Guilhem Saurel, Gabriele Buondonno, Joseph Mirabel, Florent Lamiriaux, Olivier Stasse, and Nicolas Mansard. The pinocchio c++ library – a fast and flexible implementation of rigid body dynamics algorithms and their analytical derivatives. In *IEEE International Symposium on System Integrations (SII)*, 2019.
- Roy Featherstone. *Rigid body dynamics algorithms*. Springer, 2014.
- Rene Franke, Jorn Malzahn, Thomas Nierobisch, Frank Hoffmann, and Torsten Bertram. Vibration control of a multi-link flexible robot arm with fiber-bragg-grating sensors. In *2009 IEEE International Conference on Robotics and Automation*, pages 3365–3370. IEEE, 2009.
- Alexandra Grancharova and Tor Johansen. *Explicit Nonlinear Model Predictive Control: Theory and Applications*, volume 429. 03 2012. ISBN 978-3-642-28779-4. doi: 10.1007/978-3-642-28780-0.

- Anthony Green and Jurek Z Sasiadek. Dynamics and trajectory tracking control of a two-link robot manipulator. *Journal of Vibration and Control*, 10(10):1415–1440, 2004.
- Andreas Heckmann. On the choice of boundary conditions for mode shapes in flexible multibody systems. *Multibody System Dynamics*, 23(2):141–163, 2010.
- Alan C Hindmarsh, Peter N Brown, Keith E Grant, Steven L Lee, Radu Serban, Dan E Shumaker, and Carol S Woodward. SUNDIALS: Suite of nonlinear and differential/algebraic equation solvers. *ACM Transactions on Mathematical Software (TOMS)*, 31(3):363–396, 2005. doi: 10.1145/1089014.1089020.
- J Malzahn, M Ruderman, AS Phung, Frank Hoffmann, and Torsten Bertram. Input shaping and strain gauge feedback vibration control of an elastic robotic arm. In *2010 Conference on Control and Fault-Tolerant Systems (SysTol)*, pages 672–677. IEEE, 2010.
- Stig Moberg, Erik Wernholt, Sven Hanssen, and Torgny Brogårdh. Modeling and parameter estimation of robot manipulators using extended flexible joint models. *Journal of Dynamic Systems, Measurement, and Control*, 136(3):031005, 2014.
- Julian Nubert, Johannes Köhler, Vincent Berenz, Frank Allgöwer, and Sebastian Trimpe. Safe and Fast Tracking on a Robot Manipulator: Robust MPC and Neural Network Control. *IEEE Robotics and Automation Letters*, 5(2):3050–3057, 2020. ISSN 23773766. doi: 10.1109/LRA.2020.2975727.
- Stéphane Ross, Geoffrey J. Gordon, and J. Andrew Bagnell. A reduction of imitation learning and structured prediction to no-regret online learning. In *AISTATS*, 2011.
- Lorenzo Sciavicco and Bruno Siciliano. *Modelling and control of robot manipulators*. Springer Science & Business Media, 2001.
- Ahmed A Shabana. *Dynamics of multibody systems*. Cambridge university press, 2020.
- Bernardo PM Silva, Bruno A Santana, Tito LM Santos, and Marcio AF Martins. An implementable stabilizing model predictive controller applied to a rotary flexible link: An experimental case study. *Control Engineering Practice*, 99:104396, 2020.
- Peter Staufer and Hubert Gatringer. State estimation on flexible robots using accelerometers and angular rate sensors. *Mechatronics*, 22(8):1043–1049, 2012.
- W Sunada and S Dubowsky. The application of finite element methods to the dynamic analysis of flexible spatial and co-planar linkage systems. 1981.
- Abraham P. Vinod, Sleiman Safaoui, Ankush Chakrabarty, Rien Quirynen, Nobuyuki Yoshikawa, and Stefano Di Cairano. Safe multi-agent motion planning via filtered reinforcement learning. In *2022 International Conference on Robotics and Automation (ICRA)*, pages 7270–7276, 2022. doi: 10.1109/ICRA46639.2022.9812259.
- Kim Peter Wabersich and Melanie N. Zeilinger. A predictive safety filter for learning-based control of constrained nonlinear dynamical systems. *Automatica*, 129(May), 2021. ISSN 00051098. doi: 10.1016/j.automatica.2021.109597.

Edmund Wittbrodt, Iwona Adamiec-Wójcik, and Stanislaw Wojciech. *Dynamics of flexible multi-body systems: rigid finite element method*. Springer Science & Business Media, 2007.

Tsuneo Yoshikawa and Koh Hosoda. Modeling of flexible manipulators using virtual rigid links passive joints. *International Journal of Robotics Research*, 15(3):290–299, 1996. ISSN 02783649. doi: 10.1177/027836499601500305.

Appendix A. Parameters

Name	Variable	Value	Name	Variable	Value
Simulation Model			Expert MPC		
length	L [cm]	50	horizon	N	$\{10, 20, 40, 50, 80\}$
width	a [cm]	5	discr. time	Δt_{MPC} [s]	0.01
height	h [cm]	0.2	weight state	$w_{q_a}, w_{\dot{q}_a}^N$	0.01, 0.1
density	ρ [kg/m ³]	$7.87 \cdot 10^3$	weight state	$w_{\dot{q}_a}, w_{\ddot{q}_a}^N$	0.1, 1
Young’s modulus	E [Pa]	$1.9 \cdot 10^{11}$	weight state	$w_{q_p}, w_{\dot{q}_p}^N$	$10^{-3}, 10^{-3}$
shear modulus	G [Pa]	$7.4 \cdot 10^{10}$	weight state	$w_{\dot{q}_p}, w_{\ddot{q}_p}^N$	10, 10
damping ratio	ζ	$5 \cdot 10^{-3}$	weights controls	\mathbf{r}	$[0.1, 1, 1]^\top$
torque constraints	$\bar{\mathbf{u}}$ [Nm]	$[20, 10, 10]^\top$	weights alg. states	\mathbf{p}	$\mathbf{1}^3 \cdot 3 \cdot 10^3$
torque constraints	$\underline{\mathbf{u}}$ [Nm]	$-[20, 10, 10]^\top$	weights alg. states	\mathbf{p}^N	$\mathbf{1}^3 \cdot 3 \cdot 10^4$
vel. constraints	$\bar{\mathbf{q}}_a$ [rad/s]	$[2.5, 3.5, 3.5]^\top$	weights slacks L2	\mathbf{S}	$\text{diag}([10^3, 3 \cdot 10^5])$
vel. constraints	$\underline{\mathbf{q}}_a$ [rad/s]	$-[2.5, 3.5, 3.5]^\top$	weights slacks L1	\mathbf{s}	$[10^1, 10^6]^\top$
Estimator			integrator		implicit 4th order
integrator		Radau collocation	robust vel. constraint	$\delta_{\dot{q}}$ [s ⁻¹]	$\mathbf{1}^{n_q}$
\mathbf{q}_a initial cov.	\mathbf{p}_q	$10^{-2} \cdot \mathbf{1}^{3 \times 3}$	robust pos. constraint	δ_q [s ⁻¹]	$\mathbf{0}^{n_q}$
$\dot{\mathbf{q}}_a$ initia cov	$\mathbf{p}_{\dot{q}}$	$10^{-3} \cdot \mathbf{1}^{3 \times 3}$	robust EE constraint	δ_z [m]	$2 \cdot 10^{-2} \cdot \mathbf{1}^{n_z}$
\mathbf{q} process noise cov.	\mathbf{q}_q	$[10^{-4}, 10^{-3} \cdot \mathbf{1}^{n_q-1}]$	Safety Filter		
$\dot{\mathbf{q}}$ process noise cov.	$\mathbf{q}_{\dot{q}}$	$[0.1, 0.5 \cdot \mathbf{1}^{n_q-1}]$	horizon	N	20
\mathbf{q}_a meas. noise cov.	\mathbf{R}_{q_a}	$3 \cdot 10^{-4} \cdot \mathbf{1}^{3 \times 3}$	discr. time	Δt_{MPC} [s]	0.01
$\dot{\mathbf{q}}_a$ meas. noise cov.	$\mathbf{R}_{\dot{q}_a}$	$5 \cdot 10^{-1} \cdot \mathbf{1}^{3 \times 3}$	weight state	$w_{q_a}, w_{\dot{q}_a}^N$	0, 0
\mathbf{p}_{ee} meas. noise cov.	$\mathbf{R}_{p_{ee}}$	$10^{-2} \cdot \mathbf{1}^{3 \times 3}$	weight state	$w_{\dot{q}_a}, w_{\ddot{q}_a}^N$	0.01, 0.01
Simulator			weight state	$w_{q_p}, w_{\dot{q}_p}^N$	0, 0
sampling time	Δt [s]	0.01	weight state	$w_{\dot{q}_p}, w_{\ddot{q}_p}^N$	0.01, 0.01
integrator		CVODES	weights controls	\mathbf{r}_0	$[1, 1, 1]^\top$
relative tolerance	rtol	10^{-8}	weights controls	$\mathbf{r}_{\{1:N\}}$	$[1, 1, 1]^\top 10^{-5}$
absolute tolerance	atol	10^{-10}	weights alg. states	\mathbf{p}	$\mathbf{0}^3$
\mathbf{q}_a meas. noise cov.	\mathbf{R}_{q_a}	$3 \cdot 10^{-6} \cdot \mathbf{1}^{3 \times 3}$	weights alg. states	\mathbf{p}^N	$\mathbf{0}^3$
$\dot{\mathbf{q}}_a$ meas. noise cov.	$\mathbf{R}_{\dot{q}_a}$	$2 \cdot 10^{-3} \cdot \mathbf{1}^{3 \times 3}$	weights slacks L2	\mathbf{S}	$\text{diag}([10^3, 3 \cdot 10^5])$
\mathbf{p}_{ee} meas. noise cov.	$\mathbf{R}_{p_{ee}}$	$10^{-4} \cdot \mathbf{1}^{3 \times 3}$	weights slacks L1	\mathbf{s}	$[10^1, 10^6]^\top$
Imitation Learning			integrator		implicit 4th order
initial samples	n_0	$7 \cdot 10^3$	robust vel. constraint	$\delta_{\dot{q}}$ [s ⁻¹]	$\mathbf{1}^{n_q}$
update samples	n_1	$5 \cdot 10^3$	robust pos. constraint	δ_q [s ⁻¹]	$\mathbf{0}^{n_q}$
episodes	M	30	robust EE constraint	δ_z [m]	$2 \cdot 10^{-2} \cdot \mathbf{1}^{n_z}$

Table 4: Parameters